Journal Name

ARTICLE

Hybrid tantalum oxide nanoparticles from the hydrolysis of imidazolium tantalate ionic liquids: efficient catalysts for hydrogen generation from ethanol/water solutions

Received 00th January 20xx,
Accepted 00th January 20xx

DOI: 10.1039/x0xx00000x

www.rsc.org/

Virgínia S. Souza,[a] Jackson D. Scholten,*[a] Daniel E. Weibel,[a] Dario Eberhardt,[b,c] Daniel L. Baptista,[c] Sérgio R. Teixeira[c] and Jairton Dupont*[a,d]

The reaction of equimolar amounts of 1-*n*-butyl-3-methylimidazolium chloride (BMI.Cl) or 1-*n*-decyl-3-methylimidazolium chloride (DMI.Cl) with $TaCl_5$ afford imidazolium tantalate ionic liquids (ILs) BMI.$TaCl_6$ **1** and DMI.$TaCl_6$ **2**. The hydrolysis of ILs **1** and **2** yields hybrid-like tantalum oxide nanoparticles (NPs) with size distribution dependent on the nature of the IL used (3.8-22 nm from IL **1** and 1.5-6 nm from **2**). A significant aggregation/agglomeration of the particles was observed after the removal of the IL content of the hybrid material by calcination, forming predominantly large particles (mainly bulk tantalum oxides). These new hybrid-like Ta_2O_5/IL NPs are highly active photocatalyst nanomaterials for hydrogen production by reforming of ethanol at ambient temperature. Hydrogen evolution rate up to 7.2 mmol $H_2.g^{-1}.h^{-1}$ and high apparent quantum yields up to 17% were measured. The hybrid-like Ta_2O_5/IL NPs sputtered-decorated with ultra-small Pt NPs (1.0 ± 0.3 nm) as co-catalysts reached activities for hydrogen production even higher (9.2 $H_2.mmol.g^{-1}.h^{-1}$; apparent quantum yield of 22%). The calcined materials (with or without Pt NPs) showed much lower photocatalytic activity under the same reaction conditions (up to 2.8 $mmol.g^{-1}$ of H_2). The remarkable activity of the hybrid-like Ta_2O_5/IL NPs may be related to the presence of the remaining IL that provides hydrophilic regions, facilitating the approach of polar molecules (water and alcohol) to the semiconductor active photocatalytic sites.

Introduction

Doubtless, the size and shape controlled synthesis of metal oxide semiconductors is a key factor behind the production of hydrogen by water photocatalysis becoming a reality.[1-3] Indeed, hydrogen production with solar energy is at the center of technical solutions, in particular with the use of Ti oxides and derivative nanoparticles (NPs). Tantalum oxide and the tantalates form another large family of water splitting catalysts, but because of their large band gaps (3.9–4.0 eV for Ta_2O_5), UV irradiation is needed for activity, and in many cases, metal or metal oxide co-catalysts.[4, 5]

Ionic liquids (ILs), in particular those based on the 1,3-dialkylimidazolium cation, have proven to be a suitable media for the preparation and stabilization of a plethora of inorganic nanomaterials by either chemical or physical methods.[6-8] This is most probably the result of their pre-organized structures with polar and non-polar domains, mainly through hydrogen bonds displayed by these ILs, which induce structural directionality (entropic effect).[9] ILs have thus been used for the generation of various Ti-based nanomaterials[10-13] with high specific areas and the consequent enhancement of photocatalytic activities.[14] It is reasonable to assume that the structural directionality imposed by the IL can be more effective in the generation of structured nanomaterials if the metal oxide precursor is the IL itself. Moreover, the nanomaterials formed in this way may have a hybrid-like structure with the "chemical and/or physical" incorporation of the IL cation on the metal-oxide. The resulting material may display hydrophilic zones that can facilitate the approach of the water and other polar molecules to the active semiconductor photocatalytic sites and thus increase the rate of hydrogen formation. We report herein that the hydrolysis of new imidazolium tantalate ILs produces highly active water splitting photocatalysts (7.2 mmol $H_2.g^{-1}.h^{-1}$) with high apparent quantum yields (Φ_{app}) up to 17% that, in the presence of a Pt co-catalyst, can reach 9.2 mmol $H_2.g^{-1}.h^{-1}$ (Φ_{app} of 22%).

Experimental

1. General. All manipulations were conducted under argon atmosphere using dry boxes or standard Schlenk techniques.

[a] *Instituto de Química, Universidade Federal do Rio Grande do Sul - UFRGS Av. Bento Gonçalves, 9500, Bairro Agronomia, CEP 91501-970, Porto Alegre-RS, Brazil. E-mail: jackson.scholten@ufrgs.br; jairton.dupont@ufrgs.br*
[b] *Universidade de Caxias do Sul, Campus Vinhedos, Alameda João Dal Sasso, 70, Bairro Universitário, Bento Gonçalves-RS, Brazil.*
[c] *Instituto de Física, UFRGS, Av. Bento Gonçalves, 9500, Bairro Agronomia, CEP 91501-970, Porto Alegre-RS, Brazil.*
[d] *School of Chemistry, University of Nottingham, University Park, Nottingham, UK, NG7 2RD.*

Electronic Supplementary Information (ESI) available: [characterization and photocatalytic properties of the materials]. See DOI: 10.1039/x0xx00000x

Tantalum pentachloride (99.99%) was purchased from Alfa Aesar. The solvents acetonitrile (Tedia), dichloromethane (Tedia) and ethanol 95% (VETEC) were used as received. The thermal treatment of tantalum oxide NPs were carried out at 800 °C for 2 h using a heat rate of 5 °C/min. For the sputtering deposition, it was used a Pt target with purity of 99.999% (AJA/International) and argon gas (99.9999%). NMR spectra were recorded on 400 MHz Varian spectrometer at ambient probe temperature and referenced to internal TMS. The FTIR analysis of ionic adducts BMI.$TaCl_6$ (IL **1**) and DMI.$TaCl_6$ (IL **2**) was performed in a Bruker Alpha-P spectrometer. Electrospray ionization mass spectrometry (ESI-MS) was carried out in Waters micromass Q-Tof microTM instrument using standard operating conditions such as 3.85 kV capillary voltage and 25 V cone voltage (positive mode) or 3.87 kV capillary voltage and 35 V cone voltage (negative mode) and 80 °C of dessolvation gas temperature. The sample was dissolved in acetonitrile (0.01 mol/L) and then analyzed by ESI-MS. Differential scanning calorimetry (DSC) insights were studied using Q2000 TA instruments equipment with the heating rate of 10 °C/min and varying the temperature from –80 °C to 200 °C. Thermogravimetric analysis (TGA) was performed in Q50 TA TGA operating under nitrogen gas atmosphere (flux of 40 mL/min). The samples (10-15 mg) were heated until 700 °C with a rate of 20 °C/min. Transmission electron microscopy (TEM) micrographs were made using a JEOL JEM1200 EXII operating at an acceleration voltage of 80 kV and JEOL JEM2010 operating at 200 kV (CMM-UFRGS). Scanning transmission electron microscopy (STEM) and high-resolution transmission electron microscopy (HRTEM) analyses were performed with an XFEG Cs-corrected FEI Titan 80/300 microscope operating at 300 kV (INMETRO, Brazil). High Z-contrast images were acquired through STEM using a high-angle annular dark-field detector (HAADF). The typical lateral resolution was greater than 0.01 nm. In order to perform the TEM analysis, a small amount of the tantalum oxide nanoparticles was dispersed in acetone at 25 °C and then this dispersion was sonicated for 20 min. After, two drops of the dispersion were placed on a carbon coated copper grid. The nanoparticles diameter was estimated from ensembles of around 200 particles (400 counts) chosen in arbitrary areas of the enlarged micrographs. The diameters of the particles in the micrographs were measured using the software ImageJ. For scanning electron microscopy (SEM) studies, the sample (5 mg) was fixed in a carbon ribbon and analyzed in a JEOL JSM 5800 microscope operating at 20 kV (CMM-UFRGS) coupled with an energy-dispersive X-ray spectroscopy (EDS) detector. X-ray powder diffraction (XRD) patterns were obtained with X-ray diffractometer D-5000 Siemens-Bruker-AXS (40 kV, 25 mA, CuKα radiations). UV-Vis spectroscopy measurements were performed in a Varian Cary 5000 (diffuse reflectance mode) using an integrated sphere accessory and a light wavelength range between 200-800 nm. The band gap was estimated from the intercept of the absorption edge with the energy axis in the plot $(k/s)^2$ *vs* hν as reported in literature.[15, 16] Brunauer-Emmett-Teller (BET) studies were recorded using N_2 adsorption/dessorption isotherms in the II TriStar Micromeritics 3020 equipment. For the analysis, 250 mg of the sample was treated under vacuum at 150 °C overnight and then analyzed. X-ray photoelectron spectroscopy (XPS) analyses were obtained using an apparatus equipped with a hemispherical analyzer seven channeltrons (NT Omicron Gmbh, Germany). The excitation source was the Kα radiation - Al (1486.6 eV). Energy steps of 50 eV and 10 eV were used for the initial scans and the spectra of each element, respectively. The position of the signal corresponding to the C 1s was used for energy calibration (285 eV). For sputtering deposition, the system was first evacuated (4×10^{-6} mbar) in order to remove any contaminant gas. Pt (99.999%) was used as target. The sputtering was carried out using an argon pressure of 4×10^{-3} mbar at room temperature (25 °C), electric current of 61 mA and voltage of 437 V during 1 minute.

2. Synthesis of the chloride ILs. The ionic liquids (BMI.Cl, DMI.Cl) were prepared following previously reported procedure.[17, 18]

3. Synthesis of the tantalate ILs. The tantalate ILs (**1** and **2**) were prepared from the reaction of RMI.Cl (R = *n*-butyl, **1**; R = *n*-decyl, **2**) and $TaCl_5$ under argon atmosphere. In a typical procedure, BMI.Cl (1.00 g, 5.72 mmol) was added in a Schlenk tube and dried under vacuum for 3 days. Then, $TaCl_5$ (2.05 g, 5.72 mmol) was mixed with the BMI.Cl under argon (glovebox). This system was immersed in a silicon oil bath at 100 °C and the reaction was kept under stirring for 30 min to induce the formation of IL **1**. The same method was used for the preparation of IL **2**. In a Schlenk tube, DMI.Cl (1.00 g, 3.88 mmol) was added and dried under vacuum for 3 days. Then, $TaCl_5$ (1.39 g, 3.88 mmol) was mixed with the DMI.Cl under argon (glovebox) and the system was kept at 100 °C under stirring for 30 min to induce the formation of IL **2**.

4. Preparation of the hybrid-like Ta_2O_5/IL NPs. After the synthesis of the tantalate ILs, deionized water was added to the system in stoichiometric amount (5 mols) or 2.5 mols with respect to the IL (samples named IL/water 2:5 and IL/water 2:2.5, respectively). The reaction was kept under stirring for 24 h at 120 °C. In order to increase the yield of Ta_2O_5, the system was dissolved in hot acetonitrile (4 mL) and additional water (1 mL) was introduced to the solution. The white solid was isolated by centrifugation, washed with acetonitrile and dried under vacuum.

5. Photocatalytic reactions. In a typical reaction, a solution containing the NPs (8 mg), deionized water (6 mL), and ethanol (2 mL) was added to a quartz reactor of 20 mL, which was placed under sonication for 20 min. After, argon was bubbled into the solution in order to remove undesired dissolved gases. Then, the reactor containing the solution was degassed using a vacuum/argon system. Finally, the system was irradiated with unfiltered light from a Xe 300 W Cermax lamp (operating at 240 W) and the reaction temperature was kept at 25 °C. The photocatalytic activity of the tantalum oxide NPs was evaluated following the hydrogen gas generation from photocatalysis of water/ethanol solutions.

Results and discussion

The new imidazolium tantalate ILs BMI.$TaCl_6$ **1** and DMI.$TaCl_6$ **2** (Scheme 1a) have been easily prepared by simple mixing of equimolar amounts of 1-*n*-butyl-3-methylimidazolium chloride (BMI.Cl) or 1-*n*-decyl-3-methylimidazolium chloride (DMI.Cl) with $TaCl_5$ and heating to 100 °C for 30 min under argon. These air- and water-sensitive salts have been characterized by IR, NMR, ESI-MS, DSC, TGA and their main physical-chemical properties were also determined (Table S1 in Supporting Information). By IR analysis, it was possible to observe some expected bands from imidazolium cations at 3148, 2916, 2850, and 1463 cm^{-1} relating to CH stretching, the peak at 1565 cm^{-1} for the C=N group and that at 1155 cm^{-1} for C-N stretching. Moreover, the formation of the adduct may be suggested due to the appearance of an absorption band at 816-833 cm^{-1}, which is probably related to the Ta-Cl bond (see Figure S1 in Supporting Information). ^1H and ^{13}C NMR experiments showed a shift in the signals from the imidazolium cation for the RMI.$TaCl_6$ ILs when compared to the chloride starting materials, indicating the formation of the desired tantalate ILs. A solution of **1** or **2** in acetonitrile was analyzed by ESI-MS using standard operating conditions (see supporting

information). The ESI(–) spectrum for IL **1** revealed the signal centered at m/z 392.7595 corresponding to the anion $TaCl_6^-$ (Figure S3). In the positive mode, besides the signal of the BMI cation at m/z 139.1229, it is possible to observe signals from the ionic clusters $[C_2A]^+$, $[C_3A_2]^+$ and $[C_4A_3]^+$ (C is the cation and A is the anion). Similarly, for IL **2**, the $TaCl_6^-$ ion could be detected at m/z 392.7622 in the negative mode, whereas signals of the DMI cation (m/z 223.2181) and the cluster $[C_2A]^+$ were detected in the positive mode (see Figures S5-6). DSC measurements revealed that the ionic adducts **1** and **2** melt at 64 °C and 45 °C, respectively (Figure S8). Therefore, the imidazolium tantalate adducts can be regarded as ILs, since their melting points are located below 100 °C.[19] For IL **2**, the reduction in melting temperature may be explained by the increase of the aliphatic carbon chain attached to the imidazolium cation, which probably make the short range structural organization of the ions more difficult. In addition, the TGA technique showed that ILs **1** and **2** started to decompose at approximately 340 °C and 270 °C, respectively (Figure S9).

The hybrid-like Ta_2O_5/IL NPs were synthesized through the reaction of IL **1** or **2** with a desired quantity of water (2:5 or 2:2.5 IL:H_2O molar ratio) and stirred for 24 h at 120 °C (Scheme 1b). However, after this time, only a small amount of a white precipitate was observed. Analysis of the liquid phase by ESI-MS(+/-) suggests the formation of anionic $Ta_xO_yCl_z$ species, such as $TaOCl_4^-$, $[(BMI).TaO_3Cl]^-$ (for the hydrolysis of IL **1**) and $Ta_2O_3Cl_5^-$, akin to the species detected in a mixture of $TaCl_5$ and pyrrolidinium-based IL.[20] This is a strong indication that the presence of the imidazolium cation decreases the full hydrolysis rate of $TaCl_6^-$, similar to the classical organoaluminate ILs[21] or $TiCl_4$[22] in ILs. Moreover, the increasing on water concentration increases the rate of hydrolysis. The addition of an excess of water to a hot mixture of IL/acetonitrile affords almost instantaneously a white precipitate. The solid was isolated by centrifugation, washed with acetonitrile and dichloromethane, and dried under vacuum. The resulting white powder was characterized by TEM, SEM-EDS, XRD, BET, TGA and UV-Vis analysis. In fact, TEM confirmed the presence of irregular nanostructured materials with a particle size of 3.8-22 nm for the NPs prepared from the hydrolysis of IL **1** and 1.5-6 nm for those using the IL precursor **2** (Figure 1).

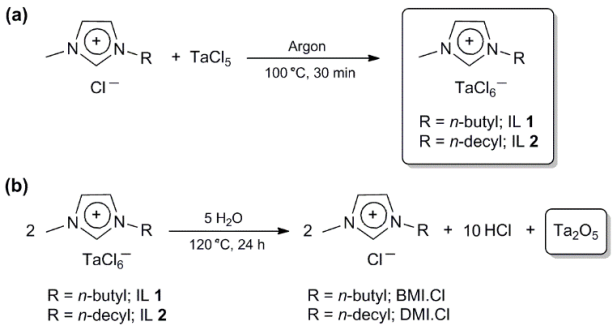

Scheme 1. Synthesis of **(a)** the imidazolium tantalate ILs **1** and **2** and **(b)** the tantalum oxide NPs.

Notably, the difference in size of the nanoparticles can be attributed to the nature of the IL used as the starting material. Indeed, the increase in the length of the alkyl side chain of the IL cation seems to control the formation and stabilization of smaller particles. Therefore, it is possible to conclude that the intrinsic properties of IL cations play an important role during the formation of the tantalum oxide nanoparticles. The crystallinity of the as-prepared hybrid-like Ta_2O_5/IL NPs was investigated by X-ray diffraction and TEM. XRD analysis revealed the existence of broad peaks, which is the typical behavior of amorphous materials or very small particles (Figure S18).

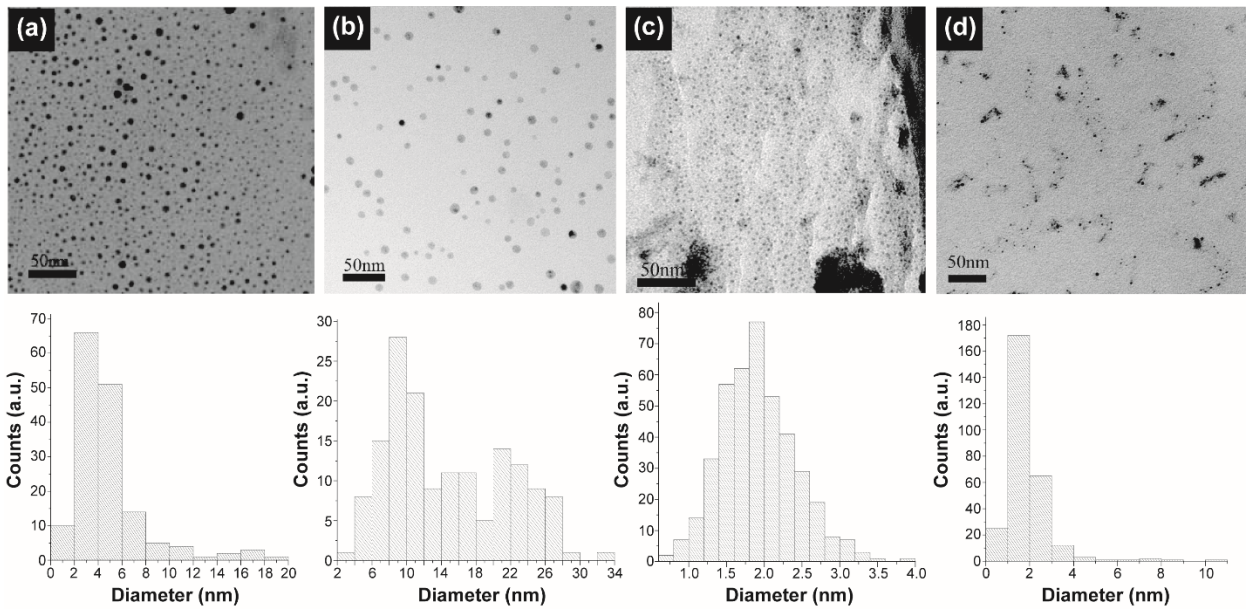

Figure 1. TEM images of the as-prepared Ta_2O_5 NPs and their size distribution: **(a)** IL **1**/water (2:2.5), **(b)** IL **1**/water (2:5), **(c)** IL **2**/water (2:2.5), **(d)** IL **2**/water (2:5). IL/water initial molar ratio.

However, using TEM (electron diffraction mode), it was possible to observe the presence of the orthorhombic crystalline structure usually observed for the tantalum oxide material (Figure S20). This result indicates that the tantalum oxide NPs are probably surrounded by an IL layer, which is responsible for the apparent broad peaks verified in the XRD technique. Indeed, this IL layer was corroborated by the presence of chloride element in the SEM-EDS and XPS[23] analyses of the as-prepared Ta_2O_5 sample, but it is probable that residual HCl[24] also remains on the particles even after washing with water (Figures S22 and S27). The IL amount present in the NPs was calculated to be in the range of 17-22% by TGA analysis (Figure S23).

The crystalline tantalum oxide NPs with the orthorhombic packing was verified by XRD after treatment at 800 °C under air for 2 h. In this case, it is important to note that the signal from the chloride element disappeared in the SEM-EDS analysis, which is expected due to the loss of the IL layer at the particles' surface after thermal treatment (see Figure S22). The band gap of the nanosized semiconductors was estimated by diffuse UV-Vis. Tantalum oxide NPs prepared from IL **1** exhibited a band gap value of 4.57-4.61 eV, whereas 4.47-4.64 eV was obtained for the samples starting from IL **2** (Figure 2). Notably, the band gap of the tantalum oxides prepared from IL **1** decreased to 4.22-4.15 eV after the thermal treatment. These results are in agreement with the size of NPs measured by TEM, since a significant aggregation/agglomeration of the particles was observed after calcination forming predominantly large ones (bulk). In fact, it is expected that bulk particles tend to possess lower band gap values.[25] Moreover, the slight change in the slope of the curve of the samples after thermal treatment in the UV-Vis analysis can be related to doping or, most probably, to the presence of defects in the crystal lattice. Interestingly, BET analysis of the as-prepared NPs revealed an unusual very low surface area (0.10-0.26 $m^2.g^{-1}$, see Table S4), which can be ascribed to the presence of the remaining IL layer surrounding the NPs' surface. Indeed, this IL layer may be responsible for the excellent photocatalytic activity exhibited by the hybrid-like Ta_2O_5/IL NPs during photocatalysis.

The photocatalytic measurements were performed in a quartz photochemical reactor under constant magnetic stirring and water filter. The use of ethanol as sacrificial agent increases considerably the hydrogen evolution rate comparing with pure water, justifying its employment.[26] Notably, previous studies on the photodecomposition of a mixture ethanol/water promoted by TiO_2 catalysts showed that the major amount of H_2 comes from the water, while a minor contribution is from ethanol.[27] To evaluate the actual role of ethanol in the H_2 production rate, the simple photolysis of ethanol under the UV light without semiconductor catalysts was performed, providing a low H_2 production (0.9 $\mu mol.h^{-1}$) under the present reaction conditions. This indicates that the water molecule may have an important role for the photocatalytic hydrogen production from alcohol/water mixtures.

In Figure 3, it is observed that the best catalytic results were obtained with the as-prepared hybrid-like Ta_2O_5/IL NPs generating up to 18 $mmol.g^{-1}$ of H_2 after 2.5 h of photocatalysis (7.2 mmol $H_2.g^{-1}.h^{-1}$) together with very low amounts of other gases (CO, CO_2 and CH_4; Table S5). For the Ta_2O_5/IL NPs prepared from IL **2**/water (2:2.5), a high Φ_{app} of 17% was determined (measured at 254 nm; see details in SI). Although higher apparent quantum yield were obtained when tantalum oxide NPs were immobilized in a conductive support, as already described for Ta_2O_5 NPs/graphene,[28] our value is

similar or even superior compared to non-supported tantalum oxide-based nanomaterials.

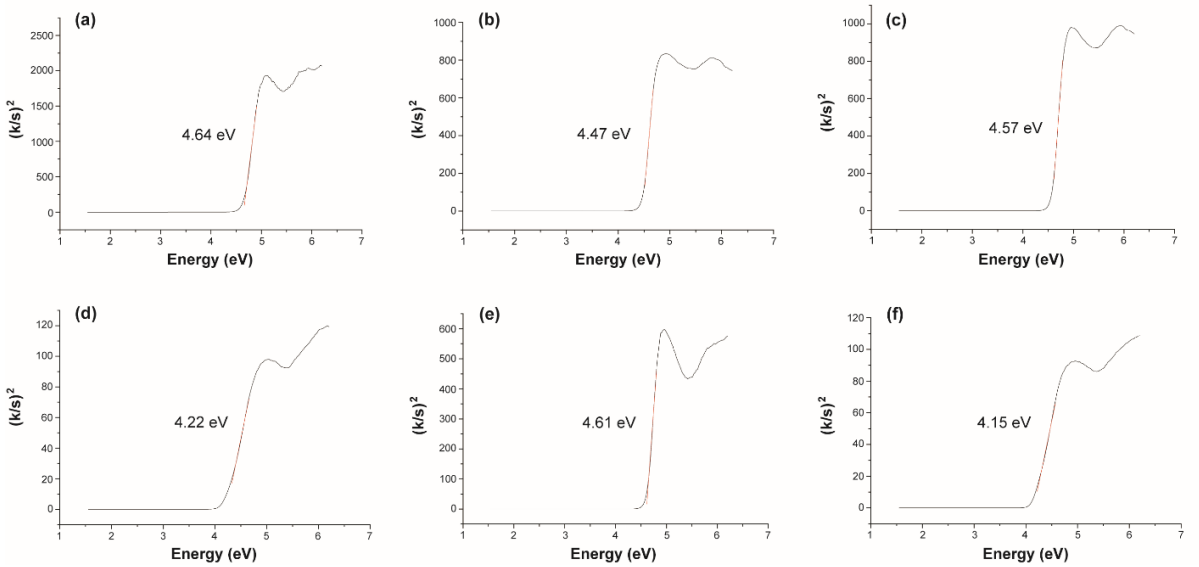

Figure 2. Diffuse UV-Vis analysis for the band gap determination of the tantalum oxide NPs prepared from the hydrolysis of **(a)** IL **2**/water (2:2.5), **(b)** IL **2**/water (2:5), **(c)** IL **1**/water (2:5), **(d)** IL **1**/water (2:5) after calcination, **(e)** IL **1**/water (2:2.5), **(f)** IL **1**/water (2:2.5) after calcination. IL/water initial molar ratio.

In contrast, after calcination, NPs showed very low activities (up to 2.8 mmol.g^{-1} of H_2) compared to the hybrid-like Ta_2O_5/IL NPs. This difference in photocatalytic activity can be related to the presence of the IL layer remaining on the surface of the as-prepared NPs, which provide hydrophilic regions that may facilitate the approach of the polar molecules (water and ethanol) to the semiconductor active photocatalytic sites, increasing the rate of H_2 formation. Other positive aspect of the prepared hybrid-like Ta_2O_5/IL NPs is their small size, which decreases the probability of electron-hole recombination allowing the electrons and holes to reach the semiconductor's surface easily. On the other hand, after calcination, the capping IL is removed from the NP's surface, which loses its favorable hydrophilic zones and aggregates into larger particles, decreasing the catalyst activity. A control experiment was performed to test the H_2 production rate when the IL is irradiated with UV light. The photodecomposition of IL **2** (2 mg) in water (8 mL) resulted in a very low hydrogen production rate (0.03 μmol.h^{-1}), indicating that the IL does not contribute significantly as co-sacrificial agent.

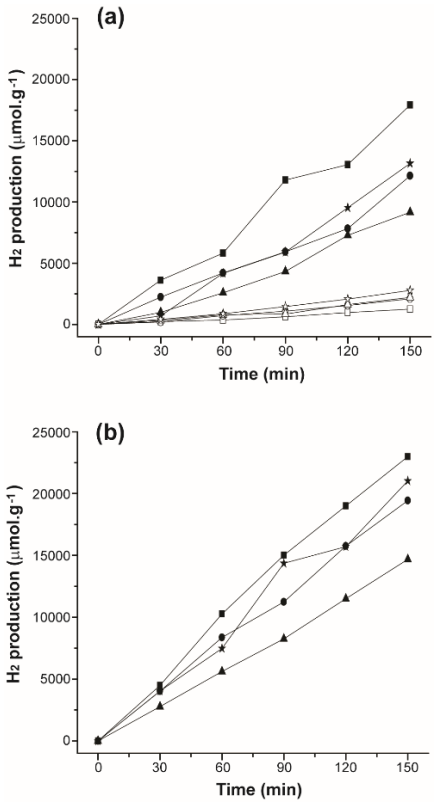

Figure 3. H_2 production from the ethanol/water mixture promoted by **(a)** tantalum oxide catalysts prepared from: (■) IL **2**/water (2:2.5), (●) IL **2**/water (2:5), (▲) IL **1**/water (2:2.5), (★) IL **1**/water (2:5), (□) IL **2**/water (2:2.5) after calcination, (○) IL **2**/water (2:5) after calcination, (△) IL **1**/water (2:2.5) after calcination, (☆) IL **1**/water (2:5) after calcination and **(b)** Pt NPs-supported tantalum oxide catalysts: (■) IL

2/water (2:2.5) with Pt, (●) IL **2**/water (2:5) with Pt, (▲) IL **1**/water (2:2.5) with Pt, (★) IL **1**/water (2:5) with Pt. IL/water initial molar ratio.

In order to enhance the catalyst activity, platinum metal NPs were deposited onto the as-prepared tantalum oxide NPs by sputtering method.[29, 30] The relative platinum content on the surface of the supported materials was estimated to be between 1.4 and 2.2% by XPS analysis (Figure S25 and Table S3). In addition, the presence of Pt NPs was confirmed by TEM measurements. Figure 4 displays the acquired images of Pt supported on the hybrid-like Ta_2O_5/IL NPs prepared from IL **2**/water (2:2.5). The presence of small Pt clusters distributed over the Ta_2O_5 support is observed by STEM-HAADF images (Figures 4a-c). The mean Pt particle size is 1.0 ± 0.3 nm, being calculated over a range of 100 particles (Figure 4e). The (111) plane of a larger and isolated *fcc* Pt particle is also observed by HRTEM (Figure 4d). The presence of Pt was also probed by spatial-resolved EDS performed in STEM. Although most characteristics EDS lines of Pt are overlapped with the Ta ones, the identification of the insulated Pt Lγ1 at 12.9 keV is an undoubted evidence of the presence of platinum (Figure 4f).

The Pt supported catalysts showed a maximum H_2 production rate of 9.2 mmol.g^{-1}.h^{-1} (Φ_{app} of 22%), which is higher than that of the catalysts without Pt (Figure 3). Notably, the Pt NPs can act as efficient traps and carriers, increasing the probability of the excited electrons reach the catalyst surface and reduce the hydrogen atoms to hydrogen gas. A control experiment without the addition of Ta_2O_5 NPs was performed to verify the influence of the Pt NPs on the hydrogen production. A mixture containing Pt NPs sputtered in IL **2** (8 mg of the mixture), ethanol (2 mL) and water (6 mL) generated only 0.08 μmol.h^{-1}, which is in agreement with previous results.[31, 32] This result indicates that the photoactivity of Pt NPs for H_2 formation is only effective after charge separation in the semiconductor (by photon absorption) coupled to the known Pt electron trapping mechanism. The synergistic effect for hydrogen photogeneration ocurred when the Pt NPs are combined with the hybrid-like Ta_2O_5/IL NPs photocatalyst.

The simple and efficient route proposed in this work for the preparation of tantalum oxide nanomaterials proved to be capable of producing one of the best active catalysts for hydrogen generation from ethanol/water photocatalysis reported to date. In fact, the activity of these photocatalysts (with or without Pt NPs) was superior when compared to other materials under similar conditions, such as tantalum oxide nanotubes (4.9 mmol $H_2.g^{-1}.h^{-1}$),[33] Ta_2O_5 doped with NiO (0.9 mmol $H_2.g^{-1}.h^{-1}$),[34] $NaTaO_3$:La (2.8 mmol $H_2.g^{-1}.h^{-1}$),[35] and tantalum-based pyrochlore/indium hydroxide nanocomposites (5.8 mmol $H_2.g^{-1}.h^{-1}$).[36] Although more active catalysts have already been reported, they normally need a mixture of doping agents to improve the photoactivity, as observed in the case of La:$NaTaO_3$.NiO.[37] However, this catalyst can suffer deactivation through the formation of nickel species. In particular, the hybrid-like Ta_2O_5/IL NPs showed unprecedented photoactivities, even in the absence of common and efficient doping agents like nickel oxide and lanthanides.

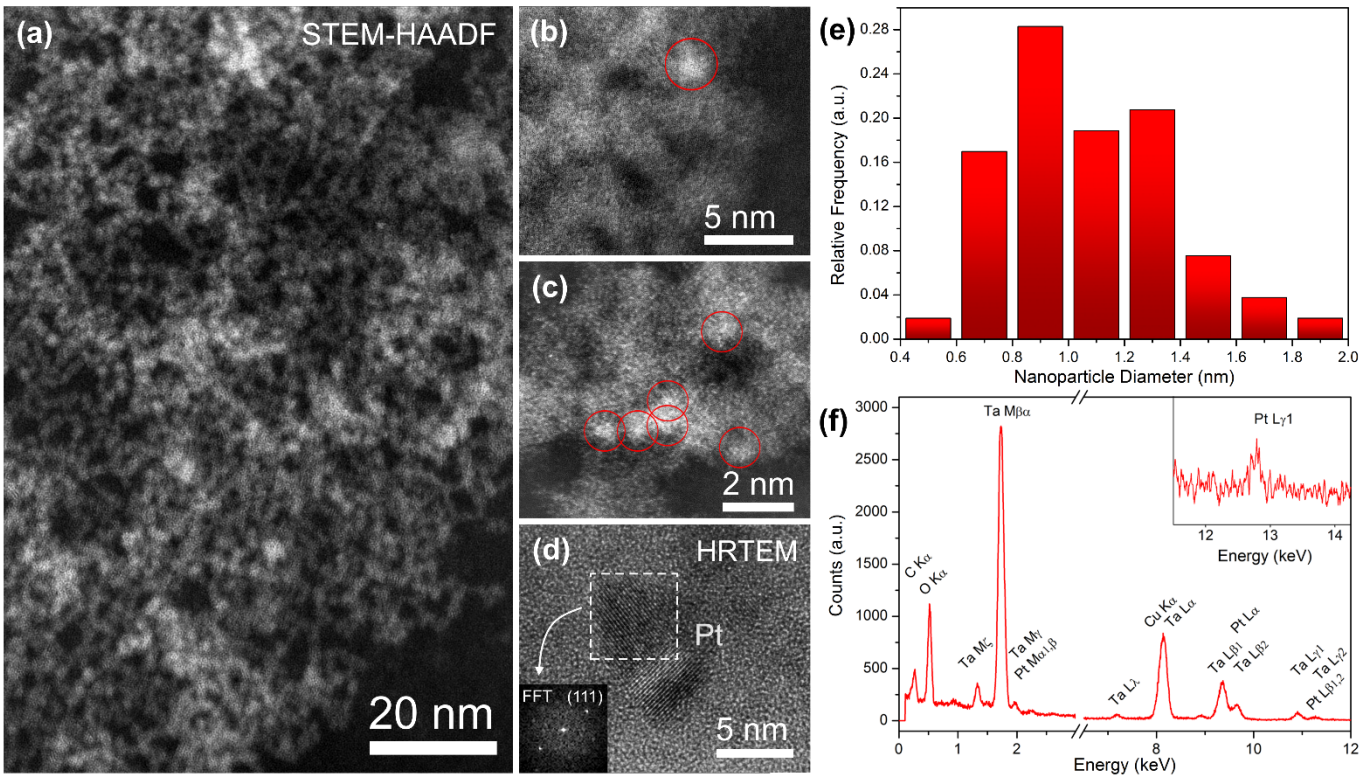

Figure 4. Selected TEM images of the supported Pt NPs onto the as-prepared hybrid-like Ta_2O_5/IL NPs (from IL **2**/water (2:2.5)): **(a-c)** STEM-HAADF images, **(d)** HRTEM image showing a *fcc* Pt particle (inset: Fast Fourier Transform (FFT) demonstrating the (111) plane of Pt), **(e)** histogram of the Pt particle size distribution (1.0 ± 0.3 nm) and **(f)** EDS analysis confirming the presence of Pt.

Conclusions

In summary, the present work describes a simple and efficient route to prepare highly active tantalum oxide photocatalysts by the hydrolysis of imidazolium tantalate ILs. This new synthetic procedure was capable of producing hybrid-like Ta_2O_5/IL NPs with size distribution dependent on the nature of the IL used. The IL cation seems to play an important role in the stabilization of NPs, since the formation of smaller particles was verified when the IL **2** (DMI cation) was employed as a precursor. Then, it is reasonable to suppose that the longer alkyl side chain in the imidazolium cation helps on the stabilization process of the nanoparticles. Notably, these nanomaterials proved to be one of the most active catalysts reported to date in the ethanol/water splitting process for hydrogen generation. The remarkable activity of these photocatalysts may be related to the presence of the remaining IL that provides hydrophilic regions, facilitating the approach of polar molecules to the semiconductor active photocatalytic sites. Moreover, the activity of the tantalum oxide NPs could be improved with the presence of Pt NPs that were deposited onto the as-prepared tantalum oxide by the sputtering method. In fact, hydrogen amounts of up to 9.2 $mmol.g^{-1}.h^{-1}$ were obtained during the photocatalysis promoted by the Pt NPs-supported tantalum oxide materials. Therefore, the new hybrid-like Ta_2O_5/IL NPs (with or without Pt NPs) reported herein can be considered exceptional highly active photocatalysts for hydrogen generation from alcohol/water solutions.

Acknowledgements

The authors thank CAPES and CNPq for the financial support. DLB thanks DIMAT/NULAM for the use of electron microscopy facilities at INMETRO (Brazil).

References

1. K. Takanabe and K. Domen, *ChemCatChem*, 2012, **4**, 1485-1497.
2. X. Chen, S. Shen, L. Guo and S. S. Mao, *Chem. Rev.*, 2010, **110**, 6503-6570.
3. F. E. Osterloh, *Chem. Mater.*, 2008, **20**, 35-54.
4. Z. Zou, J. Ye, K. Sayama and H. Arakawa, *Nature*, 2001, **414**, 625-627.
5. S. Li, S. Liu, S. Liu, Y. Liu, Q. Tang, Z. Shi, S. Ouyang and J. Ye, *J. Am. Chem. Soc.*, 2012, **134**, 19716-19721.
6. J. Dupont and J. D. Scholten, *Chem. Soc. Rev.*, 2010, **39**, 1780-1804.
7. M. Antonietti, D. B. Kuang, B. Smarsly and Z. Yong, *Angew. Chem. Int. Ed.*, 2004, **43**, 4988-4992.
8. A. Taubert and Z. Li, *Dalton Trans.*, 2007, 723-727.
9. J. Dupont, *Acc. Chem. Res.*, 2011, **44**, 1223-1231.
10. Y. Zhou and M. Antonietti, *J. Am. Chem. Soc.*, 2003, **125**, 14960-14961.
11. A. A. Ayi, V. Khare, P. Strauch, J. Girard, K. M. Fromm and A. Taubert, *Monatsh. Chem.*, 2010, **141**, 1273-1278.
12. I. Paramasivam, J. M. Macak, T. Selvam and P. Schmuki, *Electrochim. Acta*, 2008, **54**, 643-648.
13. S. E. John, S. K. Mohapatra and M. Misra, *Langmuir*, 2009, **25**, 8240-8247.
14. H. Wender, A. F. Feil, L. B. Diaz, C. S. Ribeiro, G. J. Machado, P. Migowski, D. E. Weibel, J. Dupont and S. R. Teixeira, *ACS Appl. Mater. Interf.*, 2011, **3**, 1359-1365.
15. N. B. D. da Costa, J. C. O. Pazinato, G. Sombrio, M. B. Pereira, H. Boudinov, A. Guendel, E. C. Moreira and I. T. S. Garcia, *Thin Solid Films*, 2015, **578**, 124-132.
16. V. Derstroff, J. Ensling, V. Ksenofontov, P. Gutlich and W. Tremel, *Z. Anorg. Allg. Chem.*, 2002, **628**, 1346-1354.
17. J. Dupont, C. S. Consorti, P. A. Z. Suarez and R. F. deSouza, *Org. Synth.*, 2002, **79**, 236.
18. J. S. Wilkes, J. A. Levisky, R. A. Wilson and C. L. Hussey, *Inorg. Chem.*, 1982, **21**, 1263-1264.
19. J. Dupont, R. F. de Souza and P. A. Z. Suarez, *Chem. Rev.*, 2002, **102**, 3667-3691.
20. O. B. Babushkina, S. Ekres and G. E. Nauer, *Z. Nat. Sec.-A J. Phys. Sc.*, 2008, **63**, 73-80.
21. S. Einloft, F. K. Dietrich, R. F. DeSouza and J. Dupont, *Polyhedron*, 1996, **15**, 3257-3259.
22. M. Krishnappa, V. S. Souza, N. Ganganagappa, J. D. Scholten, S. R. Teixeira, J. Dupont and R. Thippeswamy, *Chem. Eur. J.*, 2015, **21**, 17623-17630.
23. I. J. Villar-Garcia, E. F. Smith, A. W. Taylor, F. Qiu, K. R. J. Lovelock, R. G. Jones and P. Licence, *Phys. Chem. Chem. Phys.*, 2011, **13**, 2797-2808.
24. B. Pelissier, A. Beaurain, H. Fontaine, A. Danel and O. Joubert, *Microelectron. Eng.*, 2009, **86**, 1013-1016.
25. K. M. Reddy, S. V. Manorama and A. R. Reddy, *Mater. Chem. Phys.*, 2003, **78**, 239-245.
26. M. P. Languer, F. R. Scheffer, A. F. Feil, D. L. Baptista, P. Migowski, G. J. Machado, D. P. de Moraes, J. Dupont, S. R. Teixeira and D. E. Weibel, *Int. J. Hydrogen Energy*, 2013, **38**, 14440-14450.
27. T. Sakata and T. Kawai, *Chem. Phys. Lett.*, 1981, **80**, 341-344.
28. L. Mao, S. Zhu, J. Ma, D. Shi, Y. Chen, Z. Chen, C. Yin, Y. Li and D. Zhang, *Nanotechnology*, 2014, **25**, 215401.
29. T. Torimoto, K. Okazaki, T. Kiyama, K. Hirahara, N. Tanaka and S. Kuwabata, *Appl. Phys. Lett.*, 2006, **89**, 243117
30. H. Wender, P. Migowski, A. F. Feil, L. F. de Oliveira, M. H. G. Prechtl, R. Leal, G. Machado, S. R. Teixeira and J. Dupont, *Phys. Chem. Chem. Phys.*, 2011, **13**, 13552-13557.
31. P. A. Mangrulkar, A. V. Kotkondawar, S. Mukherjee, M. V. Joshi, N. Labhsetwar, D. D. Sarma and S. S. Rayalu, *Energy Environ. Sci.*, 2014, **7**, 4087-4094.
32. A. Zielinska-Jureka, Z. Wei, I. Wysocka, P. Szweda and E. Kowalska, *Appl. Surf. Sci.*, 2015, **353**, 317-325.
33. R. V. Gonçalves, P. Migowski, H. Wender, D. Eberhardt, D. E. Weibel, F. C. Sonaglio, M. J. M. Zapata, J. Dupont, A. F.

Feil and S. R. Teixeira, *J. Phys. Chem. C*, 2012, **116**, 14022-14030.
34. T. Sreethawong, S. Ngamsinlapasathian, Y. Suzuki and S. Yoshikawa, *J. Mol. Catal. A: Chem.*, 2005, **235**, 1-11.
35. H. Husin, H.-M. Chen, W.-N. Su, C.-J. Pan, W.-T. Chuang, H.-S. Sheu and B.-J. Hwang, *Appl. Catal. B-Environ.*, 2011, **102**, 343-351.
36. M.-C. Hsieh, G.-C. Wu, W.-G. Liu, W. A. Goddard, III and C.-M. Yang, *Angew. Chem. Int. Ed.*, 2014, **53**, 14216-14220.
37. H. Kato, K. Asakura and A. Kudo, *J. Am. Chem. Soc.*, 2003, **125**, 3082-3089.